Z' Model Discrimination at LHC

A. A. Nepomuceno and F. M. L. Almeida
Institute of Physics, Federal University of Rio de Janeiro
(Received on 5 June, 2008)

We study three different variables that can be useful for Z' model discrimination: the forward-backward asymmetry, the rapidity ratio and the associated production. We also present two approaches to correct the Forward-Backward Asymmetry, which is affected by the unknown initial quark direction in the proton-proton collision. The study is performed for six different Z' models, using Monte Carlo events and a fast detector simulation. It is shown that the models studied here are distinguishable for a Z' mass of 1 TeV after one year of data taking in high luminosity.

Keywords: Z'; Model discrimination

1. INTRODUCTION

It is common sense that the Standard Model (SM) is just an effective theory, and a more complex gauge structure must exist at TeV scale, since the SM does not answer various fundamental questions and there are many arbitrary parameters in the theory. To solve such problems, several scenarios have been proposed over the last 25 years, like Grand Unified Theories, 331 models, among others. All these models foresee the existence of new neutral and charged gauge bosons, generally called Z' and W', respectively. Their discovery would be clear signatures of physics beyond the SM. One of the most important goal of the LHC is to establish the model which best describe the strong and electroweek interactions.

In this paper it will be assumed that a Z' of 1 TeV mass has been discovered at LHC. One will investigate the Z' properties via the decays $Z' \longrightarrow e^+e^-$ and $Z' \longrightarrow e^+e^-\gamma$ in the context of six models and study a set of variables that can be used to identify the correct theory. The leptonic decays are preferred for this analysis because they have low background compared with hadronic searches, and their energy and momentum can be measured more precisely.

This document is organized as follows: In section 2 the models will be briefly discussed. In section 3 details on the simulation is given. Section 4 describes the variables used for model discrimination, and in Section 5 a statistical treatment is applied to the problem. The conclusions are presented in the last section

2. Z' MODELS

The most popular Z' models are effective $SU(2)_L \otimes U(1)_Y \otimes U(1)_{Y'}$ theories, which originate from the breaking of the group E_6 via $E_6 \longrightarrow SO(10) \otimes U(1) \longrightarrow SU(5) \otimes U(1) \otimes U(1)$, where the $SU(5)$ contains the SM group. Two additional neutral gauge bosons appear when the E_6 is broken down to SM, but just one of them is expected to be detected at LHC. It is defined as

$$Z' = Z'_\chi cos\beta + Z'_\psi sin\beta \qquad (1)$$

where the parameter β specifies the model. The values $\beta = 0$ and $\beta = \pi/2$ correspond to the Z'_χ and Z'_ψ models, respectively, and $\beta = arctg(-\sqrt{5}/2)$ corresponds to Z'_η model, which appears when E_6 is broken directly to a rank-5 group. For more details about E_6 breaking, see [1]. The couplings of SM fermions to the new gauge boson as a function of β can be found in [2].

Another possibility are the left-right models, which extend the SM group to $SU(2)_L \otimes SU(2)_R \otimes U(1)$ and restore the parity symmetry at high energy. In this note we will be concentrated in two kinds of left-right models with different fundamental representations : the Mirror Left-Right Model (MLRM) and the Symmetric Left-Right Model (SLRM). A detailed study of these models and the couplings between the fermions and the Z' can be found in [3].

Interesting Z' phenomenology also comes from $SU(3)_C \otimes SU(3)_L \otimes U(1)_X$ models, known as 3-3-1 models. These theories foresee new charged bosons with leptonic number two (bileptons), and in the minimal version, their mass is approximately $M_{Z'}/2$, hence Z' decay into bileptons are always kinematically allowed [4]. This model is take into account as an example of a Z' with an exotic decay. For the others models mentioned above, it is assumed that the Z' decays only into SM particles.

3. SIMULATION

The present study has been preformed by simulating the processes $pp \longrightarrow e^+e^-$ and $pp \longrightarrow e^+e^-\gamma$ (including the t-channel) at the LHC design center of mass energy of 14 TeV, with full interference between γ, Z^0 and Z'. The Z' widths and cross sections are found in Table I. The Monte Carlo program CompHep [5] was used for parton level calculation and event generation, using CTEQ6L as proton structure function. A cut on the dielectron invariant mass of $M_{ee} > 500$ GeV was applied since the current Z' lower limit is 600 - 900 GeV, depending on the model[6]. For hadronization and decays PYTHIA [7] was used. The samples were generated for an integrated luminosity of $100 fb^{-1}$, which corresponds to one year of data taking in high luminosity. A fast simulation of a typical LHC detector was applied in order to simulate the detector response.

TABLE I: Z' Mass, widths and Cross Sections.

$M_{Z'} = 1\,TeV$			
Model	$\Gamma_{Z'}$ $[GeV]$	$\sigma(pp \longrightarrow e^+e^-)$[fb]	$\sigma(pp \longrightarrow e^+e^-\gamma)$[fb]
Z'_χ	11.70	416.2	73.3
Z'_η	6.50	268.1	49.7
Z'_ψ	5.40	247.1	46.5
Z'_{SLR}	21.06	448.9	83.7
Z'_{MLR}	6.67	494.9	101.6
Z'_{331}	177.0	377.5	68.8

TABLE II: Generated and observed asymmetries at generated level.

Model	A_{FB}^{gen}	A_{FB}^{obs}	*Dilution*
Z'_χ	-0.330 ± 0.006	-0.109 ± 0.006	67%
Z'_η	-0.044 ± 0.009	-0.015 ± 0.008	66%
Z'_ψ	0.043 ± 0.009	0.021 ± 0.009	51%
Z'_{SLR}	0.258 ± 0.006	0.116 ± 0.006	55%
Z'_{MLR}	0.354 ± 0.006	0.202 ± 0.006	43%
Z'_{331}	-0.030 ± 0.008	-0.019 ± 0.008	37%

4. VARIABLES FOR MODEL DISCRIMINATION

The variables employed in this study are the forward-backward asymmetry, the rapidity ratio and the associated production ratio. Their definition and a detailed analysis of them are given in the next subsections.

4.1. The Forward-Backward Asymmetry

The forward-backward asymmetry is defined as

$$A_{FB} = \frac{N_F - N_B}{N_F + N_B} \tag{2}$$

where

$$N_F = \int_0^1 \frac{d\sigma}{dcos\,\theta^\star} dcos\,\theta^\star, \quad N_B = \int_{-1}^0 \frac{d\sigma}{dcos\,\theta^\star} dcos\,\theta^\star \tag{3}$$

The angle $\theta^\star$ is taken between the negative charge lepton and the incoming quark in the dilepton center of mass frame. For spin-1 particles, the A_{FB} can also be obtained with a fit to the $cos\theta^\star$ distribution given by

$$\frac{d\sigma}{dcos\,\theta^\star} \propto \frac{3}{8}(1 + cos^2\theta^\star) + A_{FB} cos\theta^\star \tag{4}$$

The forward-backward asymmetry provides information on the Z' couplings to the quarks and leptons, and it can be expressed in terms of the normalized couplings. Furthermore, Dittmar[8] has shown that it is almost insensitive to uncertainties in the structure function for dilepton masses above 400 GeV.

In this paper the A_{FB} is obtained in the main production channel $pp \longrightarrow e^+e^-$ and *on-peak*, which means that one takes just the events with $900 < M_{ee} < 1400\,GeV$. This invariant mass range was chosen in order to provide reasonable statistics and because it is above the interference region. The events are pre-selected by keeping two electrons with $|\eta| < 2.5$, which represents the LHC detectors acceptance, and $p_T^e > 20$ GeV.

The issue in the A_{FB} measure is that, at hadron colliders, the inicial quark direction is not known. In such case, the dilepton boost direction is taken as the quark direciton in the observed asymmetry calculation. Table II shows the generated and observed asymmetry ($A_{FB}^{gen}, A_{FB}^{obs}$) for each considered model. A_{FB}^{gen} is calculated using Equation 2 and quark direction known, with its error given by

$$\delta A_{FB}^{gen} = \frac{2}{N_T}\sqrt{\frac{N_F N_B}{N_T}} \tag{5}$$

where $N_T = N_F + N_B$, while A_{FB}^{obs} is obtained from the unbinned likelihood fit of Equation 4. The probability ν of misdetermining the quark direction is approximately 25%, and its impact on the A_{FB}^{obs} is measured by the dilution $d = 1 - A_{FB}^{obs}/A_{FB}^{gen}$. Although ν is model independent, d is strongly model dependent, as one can see in Table II, because of the different Z' couplings to the fermions.

The probability ν can be parametrized as a function of dilepton rapidity y, namely $\nu(y)$. Figure 1A shows the dilepton rapidity distribution for all the events and for those where the quark direction was wrongly determined. The ratio $\nu(y)$ between the second and the first histograms is shown in Figure 1B. As one can see, $\nu(y)$ increases as y decreases, reaching 50% at $y = 0$. This uncertainty on quark direction is due to events with low longitudinal momentum. At high rapidities values, the Z' mainly comes from the valence and the sea quark aniquilation, and the boost moves in the valence quark direction since it carries a larger momentum fraction than does the sea quark. Therefore $\nu(y) \to 0$ when y increases.

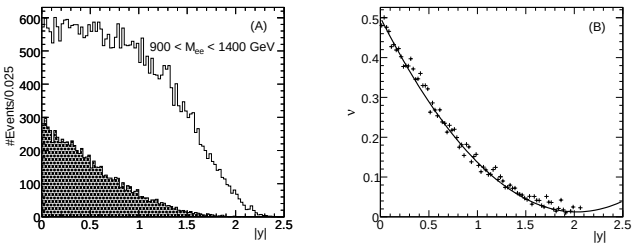

FIG. 1: (A)Rapidity distribution for all the events(clear histogram) and for those where the quark direction was misdetermined(dashed histogram). (B) Ratio between the second and the first histogram. The full line is the fit result using Equation 6.

For the ν parametrization as a function of y, one uses the expression

TABLE III: Generated and corrected asymmetries using model independent(MI) and model dependent(MD) corrections.

Model	A_{FB}^{gen}	A_{FB}^{cor} - MI	A_{FB}^{cor} - MD
Z'_χ	-0.330 ± 0.006	-0.236 ± 0.022	-0.325 ± 0.011
Z'_η	-0.044 ± 0.009	-0.045 ± 0.029	-0.048 ± 0.015
Z'_ψ	0.043 ± 0.009	0.050 ± 0.030	0.035 ± 0.016
Z'_{SLR}	0.258 ± 0.006	0.259 ± 0.020	0.263 ± 0.010
Z'_{MLR}	0.354 ± 0.006	0.391 ± 0.017	0.356 ± 0.010
Z'_{331}	-0.030 ± 0.008	-0.011 ± 0.029	-0.017 ± 0.015

$$\nu(y) = A|y|^2 + B|y| + 0.5 \quad (6)$$

where the constants A and B are obtained by fitting the $\nu(y)$ distribution from MC samples in the mass range $900 < M_{ee} < 1400\ GeV$. This information will be used to correct the asymmetry.

In order to correct the dilution effect, one can rewrite Equation 4 as

$$\frac{d\sigma}{dcos\theta^\star} \propto \frac{3}{8}(1+cos^2\theta^\star) + A_{FB}[1-2\nu(y)]cos\theta^\star \quad (7)$$

with $\nu(y)$ given by Equation 6. The unbinned likelihood fit of Equation 7 gives us the corrected asymmetries A_{FB}^{cor} and their errors as shown in Table III. Notice that, in this new fit, not only $cos\theta^\star$ but also y are input data in each event. As one can see, this approach presents a good performance in recovering the true asymmetry and has the advantage of being model independent.

Another way to correct the asymmetry is to apply model dependent correction, since the dilution is model dependent. One can get this correction by noticing that when the Z' and quark directions are opposite, one has in fact two possibilities: there is a probability ν_1 of taking an event as backward when it is forward, and a probability ν_2 of taking an event as forward when it is backward. Thus $\nu = \nu_1 + \nu_2$, and it is easy to show that the corrected asymmetry is given by

$$A_{FB}^{cor} = A_{FB}^{rec} + 2(\nu_1 - \nu_2) \quad (8)$$

Unlike ν, $\nu_{1,2}$ are strongly model dependent. The quantity $(\nu_1 - \nu_2)$ is determined from MC for each model. The goal of this method is to provide these correction factors, and, once one has the measure A_{FB}^{rec}, the different corrections can be applied to it in order to identify the underlying model. This approach can also be used as a cross-check to the model independent method described above.

The model dependent correction results are shown in the last column of the Table III. As one can see, the corrected asymmetries errors obtained with this method are about half of those from the model independent correction. In Figure 2 the true and the corrected asymmetries for both methods are compared. They show equivalent performance, but the model dependent approach presents better results for Z'_χ and Z'_{MLR} models. We have not taken into account the structure functions uncertainties in this study, and as the corrections depend on this, further investigation will be needed.

It is clear that most of the models can be well distinguished using A_{FB}^{cor}, but others like Z'_{331} and Z'_η have asymmetry values very close to each other. This problem will be discussed in more details in section 5.

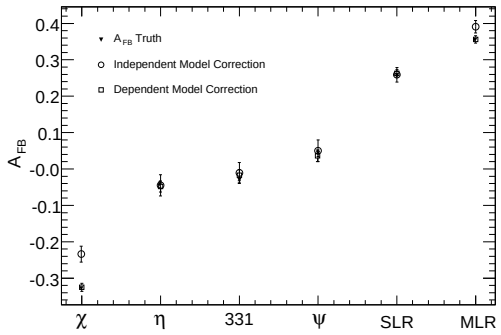

FIG. 2: True and corrected asymmetries. The triangles represet the true asymmetry, the circles the model independent correction and the squares the model dependent correction.

4.2. The Rapidity Ratio

The rapidity ratio r_{y_1} is an useful variable because it is sensitive to Z' couplings to quarks. It is defined as

$$r_{y1} = \frac{\int_{-y_1}^{y_1} \frac{d\sigma}{dy} dy}{[\int_{-y_{max}}^{y_1} + \int_{y_1}^{y_{max}}] \frac{d\sigma}{dy} dy} \quad (9)$$

where y is the dilepton rapidity. For this study the values $y_1 = 1$ and $y_{max} = 2.5$ have been chosen. The theoretical values of r_{y1} for the here considered models were numerically calculated using CompHep, and only for Z' diagram. The observed values of r_{y1} is determined by $r_{y_1}^{obs} = N_1/N_2$, where $N_{1,2}$ are the number of events in the range $|y| < 1$, $1 < |y| < 2.5$, respectively. The events were taken in the same mass window $900 < M_{ee} < 1400\ GeV$ that was used for the asymmetry studies.

In Table 4 the theoretical and observed values of r_{y1} are compared. There is a good agreement between expected and observed values, with the Z'_χ been the worst case (the reconstructed values is 1σ away from the expected). Notice that this variable provides a good discrimination for some models like Z'_χ and Z'_{SLR}, but it is not as powerful as the asymmetry. However, it can be used as a consistency check.

4.3. The Associated Production

The associated production ratio $R_{Z'\gamma}$ can be defined as

TABLE IV: Theoretical and reconstructed values of r_{y1}.

Model	r_{y1}^{theo}	r_{y1}^{obs}
Z'_χ	1.83	1.76 ± 0.07
Z'_η	1.38	1.36 ± 0.06
Z'_ψ	1.47	1.45 ± 0.06
Z'_{SLR}	1.57	1.59 ± 0.06
Z'_{MLR}	1.28	1.32 ± 0.05
Z'_{331}	1.42	1.46 ± 0.06

$$R_{Z'\gamma} = \frac{\sigma[pp \to Z'\gamma \to e^+e^-(\gamma)]}{\sigma[pp \to Z' \to e^+e^-]} \quad (10)$$

This variable has the advantage of being insensitive to the parton densities choice[9], and various systematics uncertainties are canceled out when one takes ratio of cross sections.

In this channel, the main backgrounds come from two sources: the s-channel decays $Z'/Z/\gamma \longrightarrow e^+e^-\gamma$ and jets misidentified as photons. The last background is not significant because the probability of misidentifying a jet as a photon in the LHC detectors is about 10^{-4} for jet $E_T > 40\,GeV$[10]. The first one can be removed by applying a cut on photon E_T of $E_T^\gamma > 50\,GeV$, and constraining the dielectron invariant mass in the range $999 - \Gamma_{Z'} < M_{Z'} < 1003 + \Gamma_{Z'}$, where $\Gamma_{Z'}$ is the Z' width. The t-channel events selection according to these cuts is illustrated in Figure 3 for Z'_χ model, where the reconstructed invariant mass M_{ee} is plotted for the events with two electrons and one photon in the final state. Note that the cut on photon E_T allows a good separation between s and t channel.

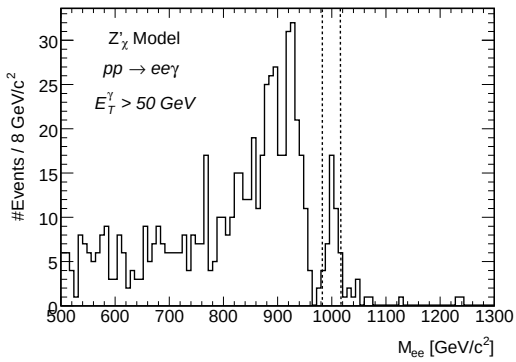

FIG. 3: t-channel events selection. A cut on photon $E_T > 50GeV$ is applied and the events are selected in the mass range $999 - \Gamma_{Z'} < M_{Z'} < 1003 + \Gamma_{Z'}$.

In order to obtain $\Gamma_{Z'}$ and $M_{Z'}$, we follow the method proposed in[11]. A function $F(M_{ll})$ is fitted to the dielectron invariant mass at reconstructed level. This function is a relativistic Breit-Wigner with multiplicative and additional exponentials that take into account the Drell-Yan background

$$F(M_{ll}) = \frac{AM^2\Gamma_{Z'}^2}{(M_{ll}^2 - M_{Z'}^2)^2 + \Gamma_{Z'}^2 M_{Z'}^2} e^{-BM_{ll}} + Ce^{-DM_{ll}} \quad (11)$$

TABLE V: Fitted $\Gamma_{Z'}$ and $M_{Z'}$. The theoretical values are found in Table 1.

Model	$M_{Z'}^{obs}$ [GeV]	$\Gamma_{Z'}^{obs}$[GeV]
Z'_χ	1001.4 ± 0.1	13.68 ± 0.25
Z'_η	1001.6 ± 0.1	8.35 ± 0.28
Z'_ψ	1001.6 ± 0.1	8.10 ± 0.26
Z'_{SLR}	1000.8 ± 0.1	22.58 ± 0.36
Z'_{MLR}	1000.9 ± 0.1	8.80 ± 0.16
Z'_{331}	1013.4 ± 0.9	150.48 ± 3.53

TABLE VI: Theoretical and reconstructed values of $R_{Z'\gamma}$.

Model	$R_{Z'\gamma}^{theo} \times 10^3$	$R_{Z'\gamma}^{obs} \times 10^3$
Z'_χ	2.8	3.1 ± 0.5
Z'_η	4.8	4.7 ± 0.9
Z'_ψ	4.0	3.9 ± 0.8
Z'_{SLR}	4.2	5.7 ± 0.6
Z'_{MLR}	5.2	5.6 ± 0.6
Z'_{331}	5.7	12.2 ± 0.9

where A,B,C,D,$M_{Z'}$ and $\Gamma_{Z'}$ are the fitted parameters. The Z' widths and masses obtained for all the models are shown in Table V.

The denominator in Equation 10 is estimated in the channel $pp \longrightarrow e^+e^-$ by the difference between the total number of events selected and the number expected for the SM, *i.e.*, $N(pp \to Z' \to e^+e^-) \cong N_{total} - N_{SM}$, where N_{total} represents all the events observed above M_{ee} = 500 GeV. In spite of interference effects, this approximation reproduces reasonably well the cross section $\sigma(pp \to Z' \to e^+e^-)$.

The variable $R_{Z'\gamma}$ is determined by the ratio between the number of events selected according to the described above for t and s channels. The theoretical and observed values of $R_{Z'\gamma}$ are compared in Table 6. Again, the theoretical values were obtained numerically.

As one can see, it is very difficult to determine $R_{Z'\gamma}$ if $\Gamma_{Z'}$ is too large, as exemplified by the 331 model. However, if the Z' width is around 10 GeV, it is possible to get a good reconstruction as one can see in Table VI for Z'_χ, Z'_η, and Z'_ψ models.

5. STATISTICAL TESTS

In the previous sections a set of variables was proposed for model discrimination. However, in order to quantify how well a model agrees with an observation, it is needed to apply statistical tests. One will use two kinds of statistical test for the present study: the Neyman-Pearson test and the χ^2 test.

5.1. The Neyman-Pearson Test

We will apply the Neyman-Pearson test to the models considered above using the forward-backward asymmetry as our measure. For details about the test, see [12]. To make the notation simpler, the reconstructed and model independent corrected asymmetry will be called a. Let us suppose, for example, that one observes $a = -0.045 \pm 0.030$. In such case, the model Z'_η could be taken as null hypothesis H_0, and the model Z'_ψ as the alternative hypothesis H_1. It will be assumed that the p.d.fs associated to each hypothesis are Gaussians centered in the true values of the asymmetries with their widths given by the experimental error $\sigma_a = 0.030$. Assuming that there is the same probability of rejecting/accepting H_0 if it is true/false (called α and β, respectivily), the cut value A^{cut} that defines the critical region is given by $A^{cut} = 1/2(A_\eta + A_\psi)$, where A_η and A_ψ are the true asymmetries for the models Z'_η and Z'_ψ, respectively. This situation is illustrated in Figure 4. As one can see, the value $a = -0.045$ lies in the acceptance region, leading us to identify Z'_η as the underlying model for the observed Z', with a power of $(1-\beta) = 93\%$. The compatibility between the observed asymmetry and the null hypothesis is measured by the P-value

$$P(A_{FB} \geq a) = \int_a^\infty Gauss(A_\eta, \sigma_a) dA_{FB} = 0.51 \qquad (12)$$

which means that one has a probability of 51% of the hypothesis H_0 be compatible with the data.

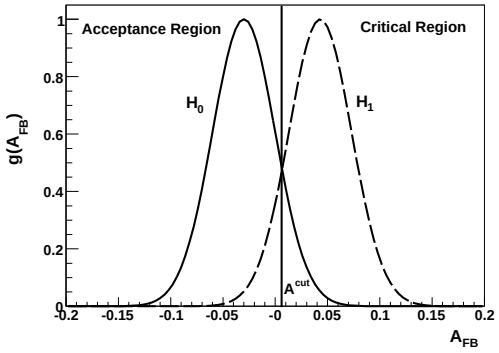

FIG. 4: Neyman-Person test for the models Z'_η and Z'_ψ. The cut values that defines the critical region is $A^{cut} = 0.0005$.

Table VII shows the power $(1-\beta)$ and the P-values for the situation where the difference between the corrected asymmetry to a prediction given by the considered models was less than 5σ. The H_0 hypothesis was always taken as that one with the true asymmetry closest to the observed a. Notice that one gets a power of discrimination around 90% for most of the tested models, and P-values greater than 45%, except for Z'_{331}. However, for the pair Z'_η/Z'_{331} this test is no longer efficient, since in this case the probability of wrongly reject(accept) H_0 is 60%. It is needed thus, apply another approach.

TABLE VII: Power of discrimination and P-values for the tested hypothesis using the Neyman-Pearson test.

Hypothesis			
H_0	H_1	$1-\beta$	P-value
Z'_η	Z'_ψ	0.93	0.51
Z'_ψ	Z'_η	0.93	0.59
Z'_ψ	Z'_{331}	0.89	0.59
Z'_{331}	Z'_ψ	0.89	0.26
Z'_{331}	Z'_η	0.41	0.26
Z'_η	Z'_{331}	0.41	0.51
Z'_{SLR}	Z'_{MLR}	0.99	0.48
Z'_{MLR}	Z'_{SLR}	0.99	0.98

5.2. The χ^2 test

Instead of testing a single value using different variables as was done before, one can compare a given distribution for two different models and compute a χ^2 value for them. For this task, it will be used the dilepton rapidity distribution and a χ^2 function given by[13]

$$\chi^2 = \sum \chi_i^2 = \sum 2(k_i - n_i) + (2n_i + 1)\ln\left(\frac{2n_i+1}{2k_i+1}\right) \qquad (13)$$

This χ^2 was chosen because it shows better performance than the usual one, even for low bin content or when the bin content is zero. This test consist in comparing two rapidity distributions from different models and calculating the χ_i^2 in each bin, where n_i and k_i are the number of events in the i^{th} bin in each correspondent distribution. A larger χ^2 corresponds to larger discrepancies between the models. The probability of the two histograms be compatible is given by the P-value

$$P = \int_{\chi^2}^\infty f(z; n_d) dz, \qquad (14)$$

where $f(z; n_d)$ is the χ^2 distribution and n_d is the number of degrees of freedom or the number of bins when one compares histograms. If $P \to 0$, the histograms are incompatible, but if $P \to 1$, one says that they are compatible and there is no significant difference between the models.

Figure 5 shows the reconstructed dilepton rapidity distributions for the models Z'_η and Z'_{331}. The events were taken in the mass window $900 < M_{ee} < 1400\, GeV$ and distributed in a histogram of 100 bins. Although the histograms seem to be very similar, the χ^2 calculated for them using Equation 13 was 191.84, which give us a P-value of 10^{-9}, i.e,the histograms are statistically very distinguishable.

Notice that when one has real data, they can be compared with the predicted MC rapidity distribution for each model by applying this approach. The underlying model then is identified as that one with the greatest P-value obtained from equation Equation (14).

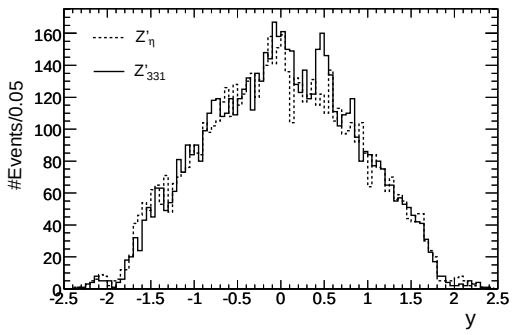

FIG. 5: Reconstructed dilepton rapidity distribution for the models Z'_η and Z'_{331}.

6. CONCLUSIONS

Methods and variables to identify the corrected SM extension if a new neutral gauge boson is found at LHC have been investigated. We have shown that the Forward-Backward asymmetry, the rapidity ratio and the associated production is a powerful set of variables for model discrimination. The approaches presented to correct the asymmetry showed good and similar results, but the model dependent correction showed better performance for Z'_χ and Z'_{MLR} models. Using the Neyman-Person test, one can distinguish the models with a power of discrimination of 90%, except the pair Z'_η/Z'_{331}. In this case a χ^2 test was applied, giving us good results. It is important to mention that the errors were calculated for an integrated luminosity of 100 fb^{-1}, and a lower luminosity will lead to bigger errors and consequently the variables sensibility to model discrimination will decrease.

Acknowledgements

This work was partially supported by the Brazilian agencies CNPq and CAPES.

[1] J. L. Hewett et al., Phys. Reports **183**, 193 (1989).
[2] A. Djouadi et al., Z. Phys. C **56**, 289 (1992).
[3] F. M. L. Almeida et al., Eur. Phys. Journal C **38**, 115 (2004).
[4] E. Ramirez et al., Phys. Lett. B **632**, 675 (2006).
[5] A. Pukhov et al., CompHep - a package for evaluation Feynman diagrams and integration over multi-particle phase space. [arXiv:hep-ph/9908288]
[6] A. Abulencia et al., Phys. Rev. Lett. **96**, 211801 (2006).
[7] T. Sjostrand, Comp. Phys. Comm. **82**, 74 (1994).
[8] M. Dittmar, Phys. Rev. D **55**, 161 (1997).
[9] T. G. Rizzo, Phys. Rev. D **47**, 956 (1993).
[10] A. Solodkov, EPJdirect C **4**, (S1) (2002).
[11] M. Schafer et al., Z' studies in full simulation, ATL-PHYS-PUB-2005-010 (2005).
[12] W. T. Eadie et al., *Statistical Methods in Experimental Physics*, North-Holland (1971) 224.
[13] F. M. L. Almeida et al., Nucl. Instrum. Meth. A **449**, 383 (2000).